




RESEARCH ARTICLE

Human-like motion planning of robotic arms based on human arm motion patterns

Jing Zhao¹ , Chengyun Wang¹  and Biyun Xie^{2,*} 

¹Faculty of Materials and Manufacturing, Beijing University of Technology, Beijing, China and ²Electrical and Computer Engineering Department, University of Kentucky, Lexington, KY, USA

*Corresponding author. E-mail: Biyun.Xie@uky.edu

Received: 31 March 2022; **Revised:** 6 August 2022; **Accepted:** 18 August 2022; **First published online:** 27 September 2022

Keywords: robot human-like motion planning, human–robot interaction, movement primitive, Rapid upper limb assessment (RULA), human arm motion pattern

Abstract

Robots with human-like appearances and structures are usually well accepted in the human–robot interaction. However, compared with human-like appearances and structures, the human-like motion plays a much more critical role in improving the efficiency and safety of the human–robot interaction. This paper develops a human-like motion planner based on human arm motion patterns (HAMPs) to fulfill the human–robot object handover tasks. First, a handover task is divided into two sub-tasks, that is, pick-up and delivery, and HAMPs are extracted for these two sub-tasks separately. The resulting HAMPs are analyzed, and a method is proposed to select HAMPs that can represent the characteristics of the human arm motion. Then the factors affecting the duration of the movement primitives are analyzed, and the relationship between the duration of the movement primitives and these factors is determined. Based on the selected HAMP and the computed duration of the movement primitives, a human-like motion planning framework is developed to generate the human-like motion for the robotic arms. Finally, this motion planner is verified by the human–robot handover experiments using a KUKA IIWA robot. It shows that the resulting trajectories can correctly reflect the relative relationship between the joints in the human arm motion and are very close to the recorded human arm trajectories. Furthermore, the proposed motion planning method is compared with the motion planning method based on minimum total potential energy. The results show that the proposed method can generate more human-like motion.

1. Introduction

With the maturity of the robot technology, robots are gradually applied to industries, entertainment, and other fields where the human–robot interaction is frequently preferred. These interactions require robots to mimic humans not only in appearance and structure but also in behavior, action, and motion. In particular, the human-like motion of robotic arms can help humans better understand and interpret the robot's intention, which can improve the quality of the human–robot interaction [1, 2].

The existing studies on robot human-like motion planning (HMP) can be roughly divided into three categories: HMP based on a human arm performance measure, HMP based on imitation learning, and HMP based on movement primitive. HMP based on a human arm performance measure uses human arm performance measures to represent certain characteristics of the human arm motion, and then optimizes these human arm performance measures to obtain robot motions similar to the human arm motion. Examples include the hand-jerk model, based on the smoothness of the motion trajectory [3], the torque model, based on the minimum joint torque [4], the kinetic energy and the potential energy model [5], the time base generator model [6]. In ref. [7], the human-like end trajectory is obtained based on the jerk model. The optimal human-like arm posture is obtained by minimizing the total potential energy. In ref. [8], task-dependent hierarchy of spatial and postural constraints are modeled as cost functions, and a human-like upper limb motion planner is proposed based on the cost functions. In ref. [9], the muscle

strength is introduced as a criterion to generate a human-like trajectory and deduced two recognition rules of geometric configurations to realize the human-like motion. However, establishing these indicators has certain subjective factors, and most focus on the trajectory of the end of the human arm. Whether the posture of the arm imitates robot motion is not considered, and it may be complicated to obtain the end trajectory from the index optimization and then solve the trajectory of the joints of the robot.

For the motion planning methods based on the imitation learning, a human demonstrates a certain action, and the robot directly imitates it. In refs. [10, 11], the basic action set is established by extracting features through multiple demonstrations, but the data dimension is high, and the versatility of the skill transfer is poor. In ref. [12], the robotic arm's human-like motion training is realized by using reinforcement learning based on a deep deterministic policy gradient and hindsight experience replay algorithm. In ref. [13], the biophysical characteristics of the human arm motion were integrated into the sampling-based motion planning to generate the human-like motion. The motion planning methods based on the imitation learning require a large enough demonstration set. When the robot performs the demonstrated motion, it looks friendly, but when the demonstration condition changes, or it is a new task, the action performed is too far removed from the human action. Moreover, most of these studies used the position information to generate the robot's human-like trajectory [14, 15].

HMP based on movement primitives has become a popular method in recent years. Giuseppe [16, 17] extracted the principal components of the joint trajectory function as the basic movement primitives through the functional principal component analysis. He reconstructed the motion trajectories of each joint based on this. Fang [18, 19] extracted six hypotheses/rules about the human arm motion to form an anthropomorphic arm motion language. The anthropomorphic arm motion language and movement primitives together form a four-layer anthropomorphic arm HMP framework. In refs. [20, 21], 16 movement primitives are proposed to express the human arm motion, and a new HMP algorithm is developed based on the selection, sorting, and quantification of primitives. In ref. [22], a motion planning method based on dynamic movement primitives combined with reinforcement learning was proposed. These methods only considered the similarity of the robot's terminal velocity waveform and the static arm posture to humans, but not the relative relationship between the joints in the human arm motion. The relative motion relationship between joints in the human arm motion is significant to the human-like performance of the robot motion and directly affects the acceptance degree of humans to the robot in the human–robot interaction.

The human–robot object handover task is a common task in the human–robot interaction. In this work, we study the problem of HMP for the robot object handover task. The main contributions of this work are as follows: (1) an index named the motion pattern composite constraint similarity index (MPCSI) is developed to select HAMP that can best represent the characteristics of the human arm motion. (2) based on the analysis of the human arm motion, a method is proposed to determine the duration of the movement primitives for a given task. (3) HMP framework that includes four main modules is developed to generate the human-like motion for the robotic arms.

The remainder of this paper is organized as follows. Section 2 introduces the human arm movement primitive and HAMP, and designs the experiment of the human arm motion data acquisition. Section 3 shows the analysis of HAMPs and the establishment of a HAMP selection method in the handover task of the human arm. Section 4 analyzes the influencing factors of each primitive duration and the relationship between the primitive duration and these influencing factors. Section 5 establishes HMP method based on HAMPs. Section 6 verifies HMP method presented in this paper. Section 7 concludes this work.

2. Background

2.1. Human arm movement primitives and motion pattern

In this paper, the human arm movement primitive is introduced to express the human arm motion intuitively. The arm posture of the human arm can be determined by the position (P) and orientation (O)

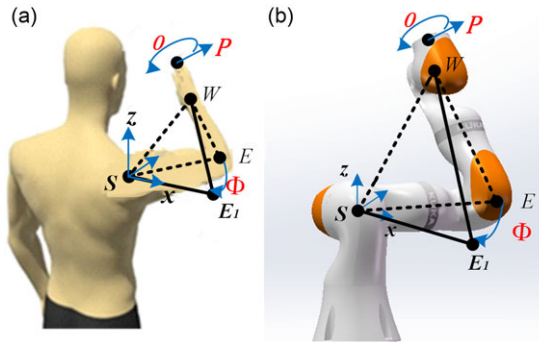


Figure 1. Expression of the human arm and the robotic arm motion. *SWE* plane is the reference plane and perpendicular to the horizontal plane. Φ is swivel angle, p and O are hand position and posture, respectively. The human arm triangle ΔSWE_1 is shown in (a). The robotic arm triangle ΔSWE_1 is shown in (b).

of the hand endpoint (fingertip), and the swivel angle (Φ). The swivel angle Φ is defined as the rotation angle of the arm triangle ΔSWE_1 around the virtual line SW , as shown in Fig. 1(a). The detailed meaning of each movement primitive is shown in ref. [18]. $\Phi(t)$, $P(t)$, and $O(t)$ can completely express the human arm motion, and are defined as the human arm movement primitive. The arm posture of the robot arm can also be represented by the corresponding movement primitive, as shown in Fig. 1(b).

These three movement primitives are also movement primitive elements that make up other movement primitives. The new movement primitive formed by these three movement primitive elements is ΦP , ΦO , PO , and ΦPO . ΦP is abbreviated of $\Phi(t)P(t)$. Other movement primitives are abbreviated according to the same rules.

So far, seven movement primitives have been proposed. The motion meanings of these assembled human arm movement primitives can be obtained by combining the motion meanings of three movement primitive elements. For instance, the motion meaning of ΦP is the combination of the motion meanings of Φ and P , that is, at time t , the arm triangle is rotating around the virtual axis, and the fingertip position also changes.

The arrangement and combination of the movement primitives expressing the motion of the human arm are defined as HAMP. For example, the primitive types of a certain motion are arranged in chronological order as follows [23]:

$$\underbrace{\Phi PO \dots \Phi PO}_k \underbrace{PO \dots PO}_m \tag{1}$$

As the primitive types of the first k frames are all ΦPO , and the remaining m frame primitives are all PO . In this case, HAMP can be abbreviated to ΦPO - PO . Other HAMPs are abbreviated according to the same rules.

2.2. Generation of the human arm motion data set

The robot object handover task can be divided into two sub-tasks: pick-up and delivery. We designed experiments to let human participants fulfill the pick-up and delivery tasks and generate a human arm motion data set for extracting the human arm motion features. In the pick-up task, the experimental scene setting is the same as in ref. [18]. The human arm rests on the right side of the body, as shown in Fig. 2(a), and the target point position distribution is shown in Fig. 2(b). The distance between adjacent points is 10 cm, and there are 108 target points in total. At the end of the pick-up task, the tip of the right finger pointed to the marked point in Fig. 2(a). Ten participants participated in this experiment. Each target point was repeated three times. A total of 3240 experiments were completed.

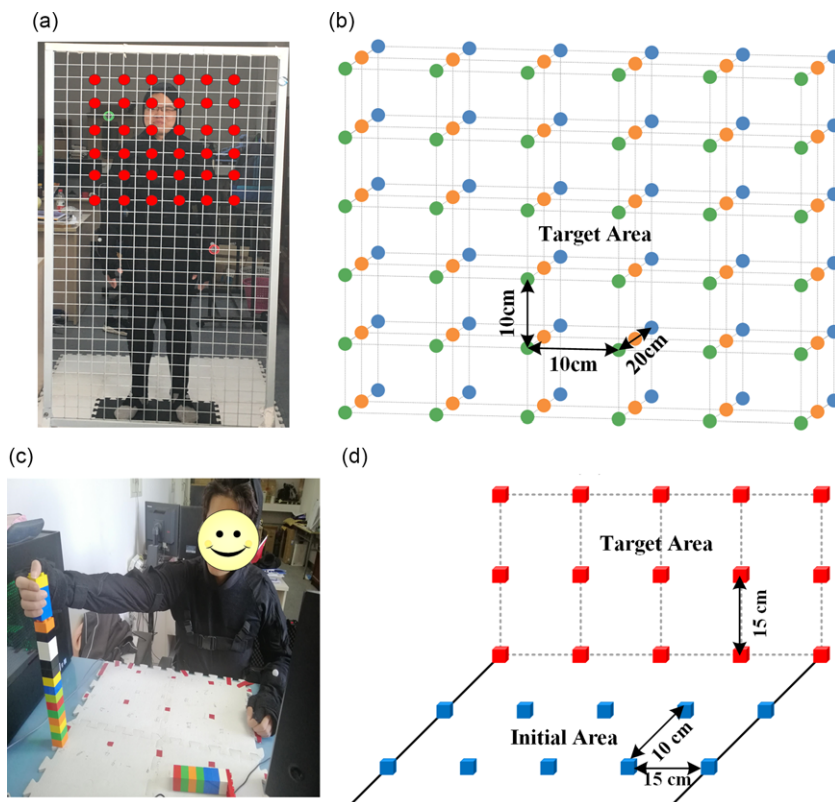


Figure 2. The pick-up sub-task experimental scene and the target point distribution are shown in (a) and (b), respectively. The delivery sub-task experiment scene and the starting and target points distribution are shown in (c) and (d), respectively.

In the delivery motion, the starting position of the human arm is 10 mark points in the initial area of Fig. 2(d), and the target position of the human arm is 15 mark points in the target area. In the experiment, the participants are required to place their right hand naturally at the starting point and then move their hands to the target point at a natural speed and a more comfortable rhythm befitting daily life, as shown in Fig. 2(c). Eleven participants participated in the delivery task experiment, each participant performed 450 experiments, and a total of 4950 experiment data points were collected.

Before collecting experimental data, each participant conducted several pre-experiments to become familiar with the experimental content. During the experiment, each participant wore motion capture clothing that recognized arm motions. OptiTrack motion capture system collects the data of the human arm motion of each participant at a rate of 120 Hz.

According to the definition of HAMP, HAMP extraction algorithm is as follows. (1) Extract right arm motion data from the collected human BVH data. (2) Calculate the values of primitives Φ , P , and O in each frame of data. (3) Identify the human arm movement primitives in each frame of motion. (4) Merge adjacent and identical primitives. (5) Generate HAMPs and record the duration of each primitive.

3. Human arm motion pattern analysis of object handover task

3.1. Extracting human arm motion patterns from the human arm motion data set

HAMPs of all experimental samples in the pick-up task and the delivery task are extracted and analyzed. The analysis results show 84 and 95 HAMPs for the pick-up and the delivery tasks, respectively.

Table I. The Top Five HAMPs.

No.	Pick-up	Ratio(%)	Delivery	Ratio(%)
1	ΦPO-PO	19.31	PO-ΦPO-PO	17.47
2	P-ΦPO-PO	16.54	ΦPO-PO	12.38
3	ΦP-ΦPO-PO	14.28	ΦPO	10.09
4	ΦPO-PO-ΦPO-PO	11.19	PO-ΦPO	9.98
5	P-ΦPO-PO-ΦPO	5.42	ΦPO-PO-ΦPO	8.35

Table II. Pick-up: The top five HAMPs in each phase.

No.	Phase 1	Ratio(%)	Phase 2	Ratio(%)
1	ΦPO	45.43	ΦPO-PO	63.40
2	ΦP-ΦPO	16.70	ΦPO-PO-ΦPO-PO	18.39
3	P-ΦPO	14.19	ΦPO-PO-ΦPO	4.69
4	PO-ΦPO	4.97	PO-ΦPO-PO	4.59
5	ΦPO-PO-ΦPO	4.11	ΦPO	1.59

Table III. Delivery: The top five HAMPs in each phase.

No.	Phase 1	Ratio(%)	Phase 2	Ratio(%)
1	PO-ΦPO	36.34	ΦPO-PO	41.20
2	ΦPO	31.61	ΦPO	25.00
3	ΦPO-PO-ΦPO	9.22	ΦPO-PO-ΦPO	10.71
4	ΦPO-PO	5.45	ΦPO-PO-ΦPO-PO	8.52
5	P-PO-ΦPO	3.63	PO-ΦPO-PO	3.96

The top five HAMPs in the pick-up task and the delivery task are shown in Table I. There are more HAMPs in the arm motion, and the frequency of each HAMP is lower.

As there are many types of HAMPs in the whole moving process, the frequency of each HAMP is lower, and HAMPs calculated in this way are not convenient for nuanced analysis. The study shows that the primitive P has a symmetrical bell-shaped velocity profile [3]. To make HAMP more accurately applied to the robot’s human-like motion, the human arm point-to-point motion is divided into two motion phases based on the speed peak of the primitive P.

HAMP of each motion phase is extracted and statistically analyzed separately. The statistical analysis reveals 26 and 23 types of HAMPs, respectively, in the pick-up task’s first and second motion phases. There are 16 and 21 types of HAMPs in the first and second motion phases of the delivery task, respectively. Tables II and III only show the top five HAMPs of each motion phase in the two tasks. Tables II and III show that there are relatively few types of HAMPs in each phase. Some HAMPs have a higher frequency, such as ΦPO-PO in phase 2 of the pick-up task. The results indicate that dividing the whole motion into two motion phases to analyze HAMP of each motion phase is better than analyzing HAMP of the whole motion.

3.2. Selecting the most representative human arm motion patterns

The human arm motion process is divided into two phases, and each motion phase’s HAMPs are analyzed separately to obtain representative HAMPs. However, there are still many types of HAMPs. It is necessary to select one or two HAMPs that can represent the motion characteristics of the human arm from among multiple HAMPs. In this section, combined with the frequency of HAMPs, the connection

frequency of primitives, and the primitive types and the order, we propose a motion pattern composite constraint similarity index (MPCSI) to choose HAMPs.

a) Primitive connection type: Based on the analysis of HAMPs, there are four primitive types ΦPO , ΦP , PO , and P , in all HAMPs. The different combinations of these four primitives form different types of HAMPs. Therefore, the pairwise combination of these four primitives or a single primitive is defined as the connection type of the primitives, such as ΦPO -, ΦPO - ΦP , and P -.

According to the definition of the primitive connection type, the frequency calculation formula of the primitive connection type is

$$f_{L_j} = \sum_{i=1}^{n_0} (N_{ij} f_{mi}) / \sum_{i=1}^{n_0} (N_{ci} f_{mi}) \quad (2)$$

where f_{L_j} is the frequency of the j -th primitive connection type, n_0 is the number of HAMP types, N_{ij} is the number of the j -th connection type in the i -th HAMP, f_{mi} is the number of the i -th HAMPs, and N_{ci} is the number of the primitive connection types in the i -th HAMP.

b) Motion pattern composite constraint similarity index: From the definition of HAMP, it can be seen that the primitive type and the order reflect the difference of each HAMP. The smaller the degree of change of the primitive type and the order of different HAMPs, the higher the degree of similarity. Inspired by the definition of string similarity [24, 25], it is proposed to use HAMP similarity index to measure the degree of similarity of HAMP.

Suppose one of the two HAMPs is the original HAMP, s , and the other is the target HAMP, h ; s is composed of m primitives, and h is composed of n primitives. The calculation formula of the similarity index $\text{sim}(h, s)$ of the two HAMPs can be defined as

$$\text{sim}(h, s) = \frac{n + m - d(h, s)}{n + m} \quad (3)$$

where $d(h, s)$ is the number of primitive types and sequence changes in the two HAMPs. The cost of changing what once is 1. The total number of minimum changes can be calculated by the Levenshtein distance algorithm [24].

HAMP similarity index considers the primitive types and the primitive order factors (internal factors) contained in HAMP. However, the influence of the frequency of HAMP and the frequency of the primitive connection type (external factors) on the choice of HAMP is not considered.

MPCSI solved the problem that HAMP similarity did not consider the influence of HAMP and the frequency of the primitive connection type on HAMP similarity. According to the above analysis, each HAMP contains one or more primitive connection types, and the frequency of each primitive connection type is different. Therefore, the frequency of the primitive connection type is introduced in HAMP similarity to reflect the influence of the primitive connection type on HAMP selection. The frequency of the primitive connection type is used to measure the cost of changing the primitive type and order. The higher the frequency of the primitive connection type, the higher the cost of changing the primitive type and order. For example, the frequency of the second phase of the delivery task primitive connection type ΦPO - ΦP is 0.5535, and the cost of changing the primitive connection type ΦPO - ΦP is 0.5535. Similarly, the higher the frequency of the target HAMP, the smaller the cost of changing the original HAMP.

Based on the above analysis and the formula of HAMP similarity index, MPCSI formula $\text{simc}(h, s)$ is computed under the compound constraint of the primitive connection type frequency and HAMP frequency:

$$\text{simc}(h, s) = (m + n - (1 - f_h) \sum_{j=1}^{n_c} (a_j f_{L_j})) / (m + n) \quad (4)$$

where n_c is the number of the primitive connection type. $a_j = 1$, when the j -th primitive connection type is changed from original HAMP to target HAMP, otherwise $a_j = 0$. m and n are the number of

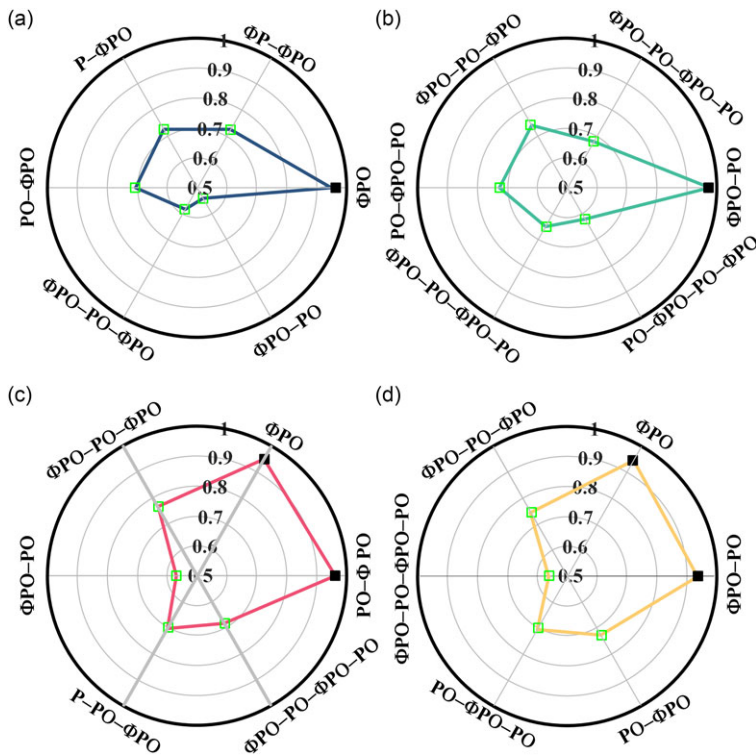


Figure 3. MPCSI values of HAMPs in the first and second phases of the pick-up task are in (a) and (b), respectively. MPCSI values of HAMPs in the first and second phases of the delivery task are in (c) and (d), respectively. The black boxes are the most representative HAMPs.

primitives contained in the original HAMP and the target HAMP, respectively; f_h is the frequency of the target HAMP.

Equation (4) is used to calculate MPCSI between HAMPs.

$$Sm = \begin{bmatrix} \text{simc}(h_1, s_1) & \text{simc}(h_1, s_2) & \cdots & \text{simc}(h_1, s_K) \\ \text{simc}(h_2, s_1) & \text{simc}(h_2, s_2) & \cdots & \text{simc}(h_2, s_K) \\ \vdots & \vdots & \cdots & \vdots \\ \text{simc}(h_L, s_1) & \text{simc}(h_L, s_2) & \cdots & \text{simc}(h_L, s_K) \end{bmatrix} \tag{5}$$

where K is the number of original HAMPs, and L is the number of target HAMPs.

$$\overline{Sm}(h_i, s) = \sum_{i=1}^K Sm(j, i)/K \tag{6}$$

where $\overline{Sm}(h_i, s)$ is the average of MPCSI between the target HAMP, h_i , and all of the original HAMPs.

The developed MPCSI is employed to select HAMP of each motion phase of the pick-up task and the delivery task. According to (6), the average value of MPCSI of HAMPs in each motion phase of the two sub-tasks is calculated, and the results are shown in Fig. 3. The figure only shows the average similarity value of the first six HAMPs of the calculation result. The higher the similarity value, the higher the degree of similarity between HAMP and other HAMPs, and the more representative the motion characteristics of the human arm.

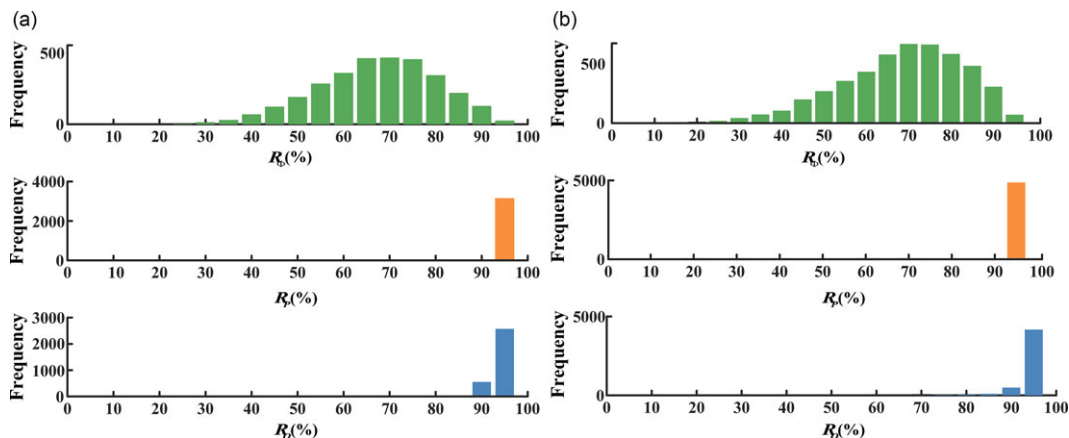


Figure 4. The primitive duration to the total duration ratio statistics. The horizontal axis shows the ratio of primitive duration to the total duration. The pick-up task and delivery task are shown in (a) and (b), respectively.

In the pick-up task, HAMP with the highest MPCSI value in the first motion phase is Φ PO. HAMP with the highest MPCSI value in the second motion phase is Φ PO-PO. MPCSI values of other HAMPs are relatively low. In the delivery task, HAMPs with higher MPCSI values in the first motion phase are Φ PO and PO- Φ PO, HAMPs with higher MPCSI values in the second phase are Φ PO and Φ PO-PO, and MPCSI values of the two are close. MPCSI values of other HAMPs are relatively low, as shown in Fig. 3.

4. Determining the duration of each movement primitive element

4.1. Analyzing the affecting factors of the movement primitive duration

The ratio of the duration of primitives Φ , P, and O to the motion’s total duration is defined as R_ϕ , R_P , and R_O , respectively. Figure 4 shows that R_ϕ , R_P , and R_O in the pick-up and delivery tasks are analyzed, respectively. It can be seen from the figure that in the pick-up task and delivery task, the sample number of primitive P and O, whose duration ratio to the total duration is between 90% and 100%, is close to the total sample number. It indicates that the duration of primitive P and O is close to the total duration. In the pick-up task and delivery task, the experimental samples corresponding to R_ϕ showed a normal distribution, and most experimental samples ranged from 50% to 90%. It can be seen from Fig. 4(a) and (b) that the results of the pick-up task and delivery task are the same. Based on the analysis of HAMP and the duration of each primitive, it can be seen that the change of HAMP type is mainly caused by the change of the duration of primitive Φ .

The relationship between R_ϕ and $\Delta\Phi$ in the pick-up and delivery tasks is analyzed, as shown in Fig. 5(a) and (b). It can be seen that R_ϕ increased with the increase of the value of $\Delta\Phi$. The relationship between R_ϕ and $\Delta\Phi$ is slightly different in the pick-up task and delivery task, but the overall trend is consistent. The variation range of R_ϕ is about 15% in each interval of $\Delta\Phi$. At this point, if $\Delta\Phi$ is used to estimate R_ϕ , the estimated primitive duration is inaccurate. The wide variation range of R_ϕ is caused by the differences of experimental individuals, as shown in Fig. 5(c) and (d). There is a significant difference in the variation of R_ϕ with the change of $\Delta\Phi$ between participant 1 and participant 2.

Based on the above analysis, it can be seen that the changing trend between R_ϕ and $\Delta\Phi$ in the pick-up and the delivery task is the same. R_ϕ increases with the increase of $\Delta\Phi$. However, owing to the differences between the individuals, the value of R_ϕ within each interval of $\Delta\Phi$ varies greatly.

The individual difference is mainly reflected in the different value ranges of the primitives of the different people, which lead to the different changes in the primitives of the same motion. Therefore,

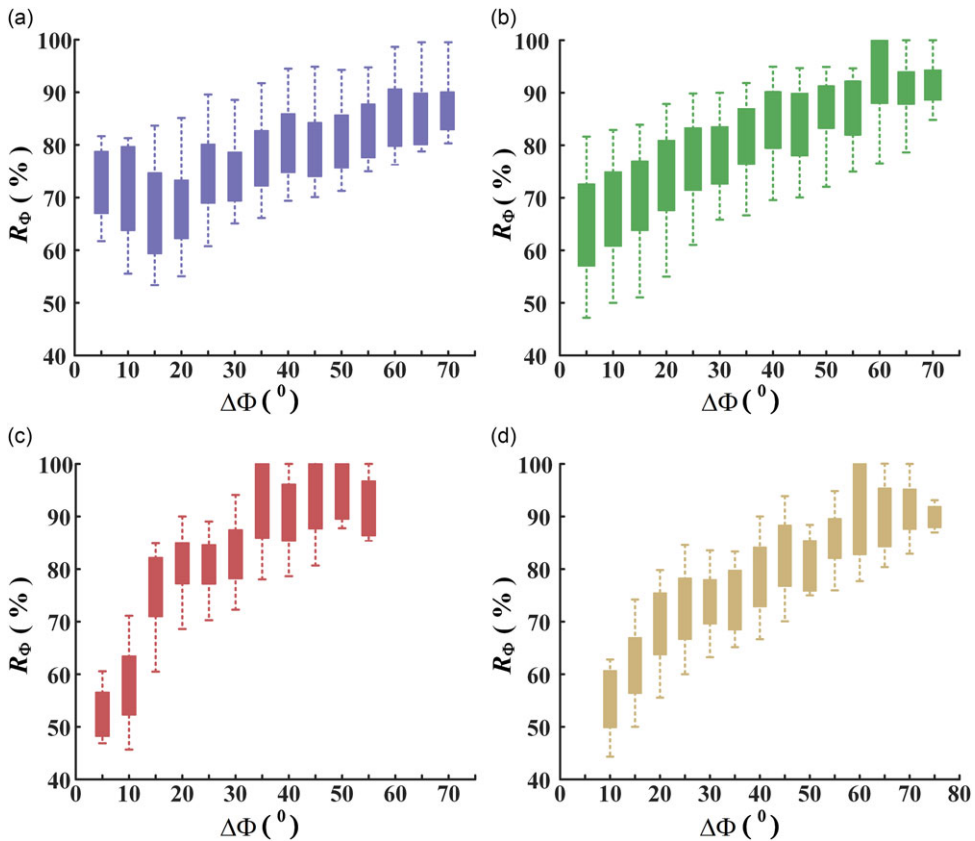


Figure 5. The statistical results of the relationship between R_Φ and $\Delta\Phi$ in the pick-up task and the delivery task are in (a) and (b), respectively. The relationship between R_Φ and $\Delta\Phi$ of participant 1 and participant 2 is in (c) and (d), respectively.

to reduce the influence of the individual differences on the value of primitive Φ duration and improve the accuracy of the estimation of the primitive Φ duration, a parameter R_d affecting the duration of the primitive Φ is introduced. R_d is defined as

$$R_d = \frac{\Delta\Phi / \Phi_M}{\Delta P / P_M} \tag{7}$$

where, $\Delta\Phi = |\Phi_f - \Phi_0|$, Φ_0 , and Φ_f are the value of primitive at the starting point and target point, respectively; Φ_M is the maximum variation range of primitive; $\Delta P = |P_f - P_0|$, P_0 , and P_f are the value of primitive P at the starting point and target point, respectively; and P_M is the maximum variation range of primitive P .

4.2. Determinate the duration of the motion primitive Φ

The duration of primitive Φ can be estimated by studying the law that R_Φ changes with R_d in the pick-up and delivery tasks of the human arm. The variation law of R_Φ with R_d is obtained through the statistical analysis of the experimental samples of the pick-up task and delivery task, as shown in Fig. 6(a) and (d), respectively. It can be seen from Fig. 6(a) and (d) that the variation range of R_Φ in the interval of R_d is about 5%. Compared with Fig. 5(a) and (b), the duration ratio of primitive Φ has a smaller range, and the duration of primitive Φ obtained by R_d is more accurate. In the pick-up and delivery tasks, the

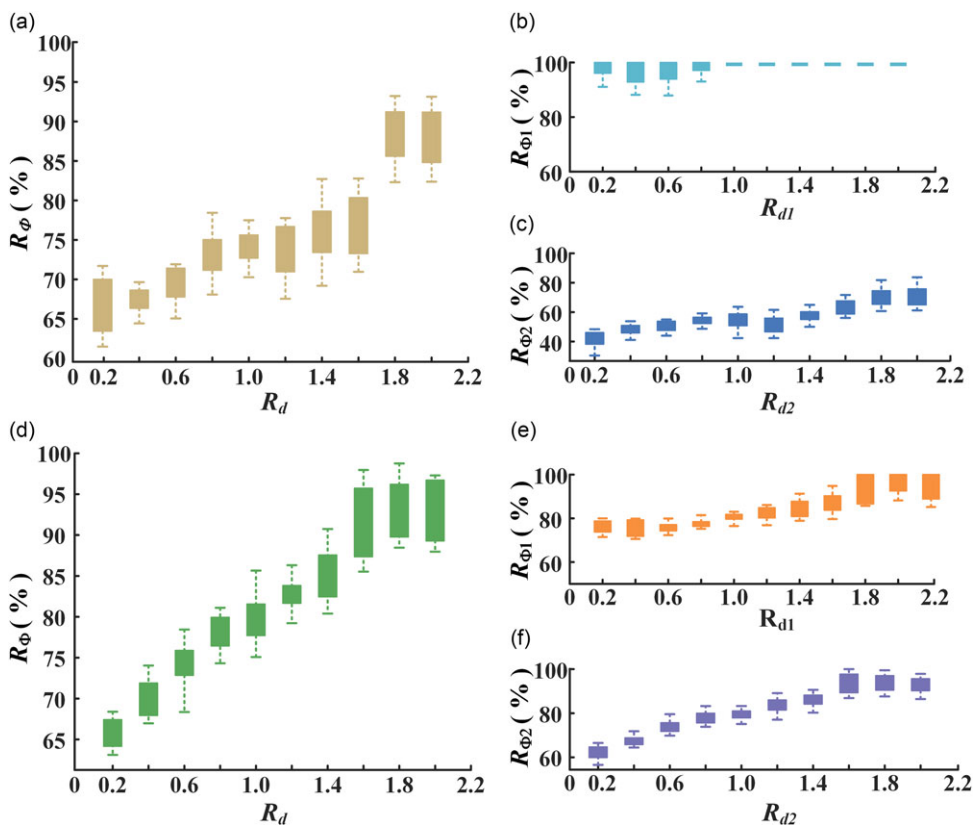


Figure 6. The relationship between R_Φ and R_d in the whole moving process and the first and second motion phases in the pick-up task is in (a), (b), and (c), respectively. The relationship between R_Φ and R_d in the whole moving process and the first and second motion phases in the delivery task is in (d), (e), and (f), respectively.

variation law of R_Φ with R_d is similar but slightly different. In the pick-up task, when $R_d \geq 1.8$, the value of R_Φ is stable at $(90 \pm 4)\%$, as shown in Fig. 6(a). In the delivery task, when $R_d \geq 1.6$, the value of R_Φ is stable at $(92 \pm 4)\%$, as shown in Fig. 6(d). The value of R_Φ no longer changes significantly with the increase of the value of R_d , and R_Φ gradually tended toward 100%. That is, the duration of primitive Φ is equal to the total duration of motion.

Figure 6(b), (c), (e), and (f), respectively, show the variation law of R_Φ with R_d in each motion phase of the pick-up task and the delivery task. It can be seen from Fig. 6(b) that the ratio R_{Φ_1} of the duration of primitive Φ to the total duration in the first phase of the pick-up task is approximately equal to 1. It shows that the duration of the primitive Φ is equal to the first phase's duration. In the second motion phase, the ratio R_{Φ_2} of the duration of primitive Φ to the total duration increases with the increase of R_{d2} , but the maximum value of R_{Φ_2} is about 80%, as shown in Fig. 6(c). The maximum duration of primitive Φ is less than the duration of the second phase. The variation law of R_{Φ_2} with R_{d2} is used to estimate the duration of primitive Φ in the second motion phase, as shown in Fig. 6(c).

In the first phase of the delivery task, when $R_{d1} \geq 1.8$, the value of R_{Φ_1} is stable at $(95 \pm 5)\%$, as shown in Fig. 6(e). It shows that the duration of the primitive Φ is equal to the first phase's duration. When $R_{d1} < 1.8$, the duration of primitive Φ is less than that of the first phase. The variation law of R_{Φ_1} with R_{d1} is used to estimate the duration of primitive Φ in the first motion phase of the delivery task, as shown in Fig. 6(e).

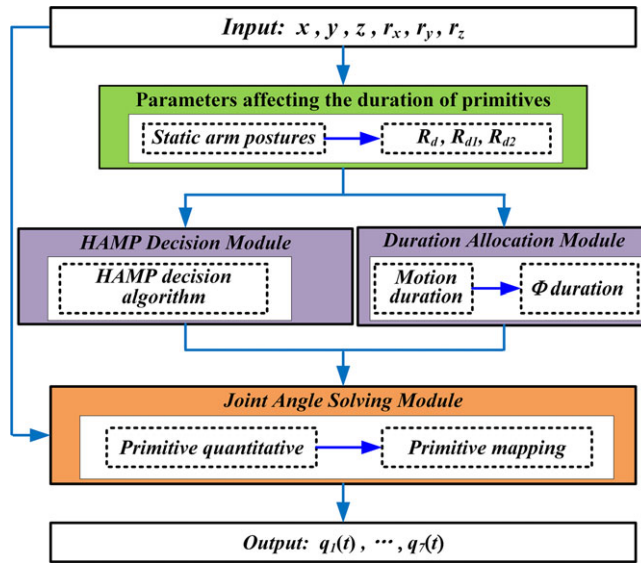


Figure 7. Motion planning framework.

In the second phase of the delivery task, when $R_{d2} \geq 1.6$, the value of R_{ϕ_2} is stable at $(93 \pm 4)\%$, as shown in Fig. 6(f). That is, the duration of primitive Φ at each phase is close to the total duration of the second phase. When $R_{d2} < 1.6$, the duration of primitive Φ is less than that of the second phase. The variation law of R_{ϕ_2} with R_{d2} is used to estimate the duration of primitive Φ in the second motion phase of the delivery task, as shown in Fig. 6(f).

5. Human-like motion planning

Based on the extracted HAMP and the relationship between the R_d and the primitive duration ratio, a new HMP algorithm is proposed. The main idea is to determine the best human-like static arm posture at the initial and target positions according to the initial posture and the target posture and calculate R_d . HAMP and the duration of the primitive are determined based on the relationship between R_ϕ and R_d . Finally, each primitive is quantified, and the mapping between the primitive and the joint angle is completed. The framework of the motion planning method is shown in Fig. 7.

5.1. Calculation of parameters affecting the duration of primitives

This module is used to calculate R_d , which provides a basis for the decision-making of HAMP and determining the duration of primitive. First, the static human-like arm posture at the starting point and the target point is calculated, and the difference $\Delta\Phi$ of the primitive Φ between the starting point and the target point is determined. Then, R_d is calculated according to (7). Finally, the motion is divided into two phases, and R_{d1} and R_{d2} are calculated for the first and the second phases according to the above method.

5.2. Human arm motion pattern decision module

This module is used to determine HAMP during the motion. In the first phase of the pick-up task, the primitives Φ , P, and O durations are close to the first phase's duration. Therefore, HAMP in the first phase of the pick-up task is ΦPO . In the second phase of the pick-up task, the primitives p and O durations are

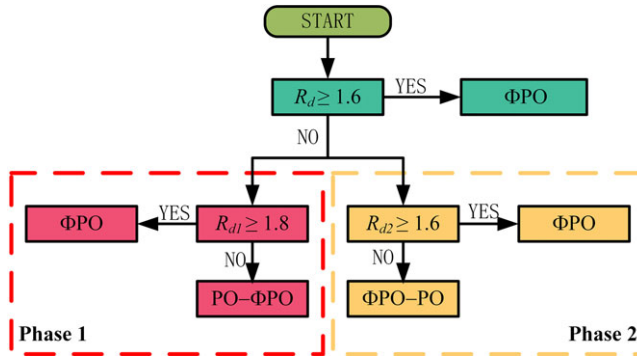


Figure 8. HAMP decision algorithm for delivery task.

close to the second phase’s duration. But, the maximum duration of primitive Φ is less than the duration of the second phase. Therefore, HAMP in the second phase of the pick-up task is Φ PO-PO.

In the delivery task, when $R_d \geq 1.6$, HAMP of the delivery task is Φ PO. When $R_d < 1.6$, the delivery task is divided into two motion phases. When $R_{d1} \geq 1.8$ and $R_{d2} \geq 1.6$, the duration of the primitive Φ is close to the total duration. Therefore, HAMP of the first phase and the second phase is Φ PO. In the same way, when $R_{d1} < 1.8$ and $R_{d2} < 1.6$, HAMP of the first motion phase and the second motion phase is PO- Φ PO and Φ PO-PO, respectively. The detailed flow of HAMP decision-making process of the delivery motion is shown in Fig. 8.

5.3. Duration allocation module

This module contains two sub-modules, the total motion duration module, and the primitive duration module. First, the total duration T is determined by Fitts’ Law [26, 27]:

$$T = a + b \log_2(2A/W) \tag{8}$$

where A is the Euclidean distance between the starting point and the target point, and W is the size of the target. Based on the experimental device in Fig. 2, W is set to 20 mm. a and b are the undetermined coefficients. According to the experimental data of Section 2.2, the values of a and b are obtained by the regression method. They are $a = 0.3625$ and $b = 0.1325$, respectively.

Then, the total duration is allocated to each primitive in HAMP. From the analysis in Section 4.1, it can be seen that the duration of the primitive P and O is equal to the total duration, so the duration of the primitive P and O is T . The principle of the duration allocation for primitive Φ is

$$T_{\Phi 1} = R_{\Phi 1} T_1 \tag{9}$$

$$T_{\Phi 2} = R_{\Phi 2} T_2 \tag{10}$$

where T_1 and T_2 are the motion duration of the first and the second phases, respectively; T_1 is the time corresponding to the peak velocity of the primitive P; $T_2 = T - T_1$. $T_{\Phi 1}$ and $T_{\Phi 2}$ are the motion duration of primitive Φ in the first and second phases, respectively; $R_{\Phi 1}$ and $R_{\Phi 2}$ are the ratios of the duration of the primitive Φ in the first and second phase to the duration of each phase. Their values depend on R_{d1} and R_{d2} , respectively.

To reflect the difference in the motion of the human arm, the values of $R_{\Phi 1}$ and $R_{\Phi 2}$ are randomly selected within the variation range corresponding to R_{d1} and R_{d2} .

5.4. Joint angle solving module

This module is the primitive quantization module. The primitives $\Phi(t)$, $P(t)$, and $O(t)$ can be quantified by the following formula [21]:

$$\hat{\Phi}(t) = \frac{A_\Phi}{2} \left(1 - \cos\left(\frac{2\pi t}{T_\Phi}\right) \right) \tag{11}$$

$$\hat{O}(t) = \frac{A_o}{2} \left(1 - \cos\left(\frac{2\pi t}{T_o}\right) \right) \tag{12}$$

$$\hat{P}(t) = (\mathbf{P}_0 - \mathbf{P}_f) (60\tau^3 - 30\tau^4 - 30\tau^2) / T_p \tag{13}$$

where $\hat{\Phi}(t)$, $\hat{P}(t)$, and $\hat{O}(t)$ are the derivatives of $\Phi(t)$, $P(t)$, and $O(t)$, respectively. T_Φ , T_p , and T_o are the duration of the primitive Φ , P , and O , respectively. $A_\Phi = 2(\Phi_f - \Phi_0)/T_\Phi$, Φ_0 , and Φ_f are the initial and end values of primitive Φ , respectively. $A_o = 2(O_f - O_0)/T_o$, O_0 , and O_f are the initial and end values of primitive O , respectively. \mathbf{P}_0 , \mathbf{P}_f is the starting point and the target point position, respectively. Moreover, $\tau = t/T_p$, $t \in [0, T_p]$.

6. Experiment

To verify the effectiveness of the proposed HMP algorithm, the object handover experiments are conducted on seven degrees of freedom (DOF) KUKA IIWA robots. At the beginning of the pick-up task, the human arm rests on the side of the body, and the robot arm has the same initial configuration. Based on the above information, HAMP and primitive duration are determined according to the motion planning algorithm proposed in Section 5. HAMP and the primitive duration between other initial points and target points in the robot workspace are determined similarly. The demonstration of the proposed motion planning method on the IIWA robotic arm proved the proposed method’s feasibility and effectiveness, as shown in Fig. 9.

Next, the human-like degree of the proposed HMP method is evaluated and compared. In this paper, the rapid upper limb assessment method (RULA) [28] is used to evaluate the human-like degree of robot motion. The scoring results are shown in Fig. 10. RULA score and the changing trend of RULA score obtained by the proposed HMP method are compared with those obtained by HMP method based on the minimum total potential energy (MTPE) method [7]. RULA is a relatively recognized simple and easy evaluation method. It evaluates the arm’s big arm, forearm, and wrist separately. The lower the score, the more beneficial it is for itself and the higher the comfort level. We used RULA to score the postures of the arm and the IIWA robotic arm. Comparing RULA score and its change trend shows the degree of the robotic arm’s human-like motion. The closer RULA score and its change trend to the human arm during the motion of the robotic arm, the higher the degree of the human-like motion during the motion of the robotic arm.

To evaluate and compare the human-like degree of HMP method, the human arm and the robot completed similar object handover tasks, namely the pick-up, and the delivery, as shown in Fig. 9. The participant wears motion capture clothes to achieve the object handover motion. The motion capture clothes record the motion data of the human arm at 120 Hz. Before the experiment, the participant’s arm rests on the side of the body. The participant naturally moved his arm to grab the object during the pick-up task. Then, the participant naturally moved his arm to the object delivery’s position (delivery task), as shown in Fig. 9(a). IIWA robotic arm in our laboratory cannot perform the same natural drooping posture as the human arm to complete the pick-up task. Therefore, to form a clear contrast with the human arm object handover experiment, V-REP software is used for the simulation experiment. HMP method proposed in this paper and HMP method based on MTPE are used to plan the robot object handover motion, respectively. The experimental process of the object handover is shown in Fig. 9(b) and (c), respectively. It can be seen from Fig. 9 that, in the object handover task, the robot posture based on

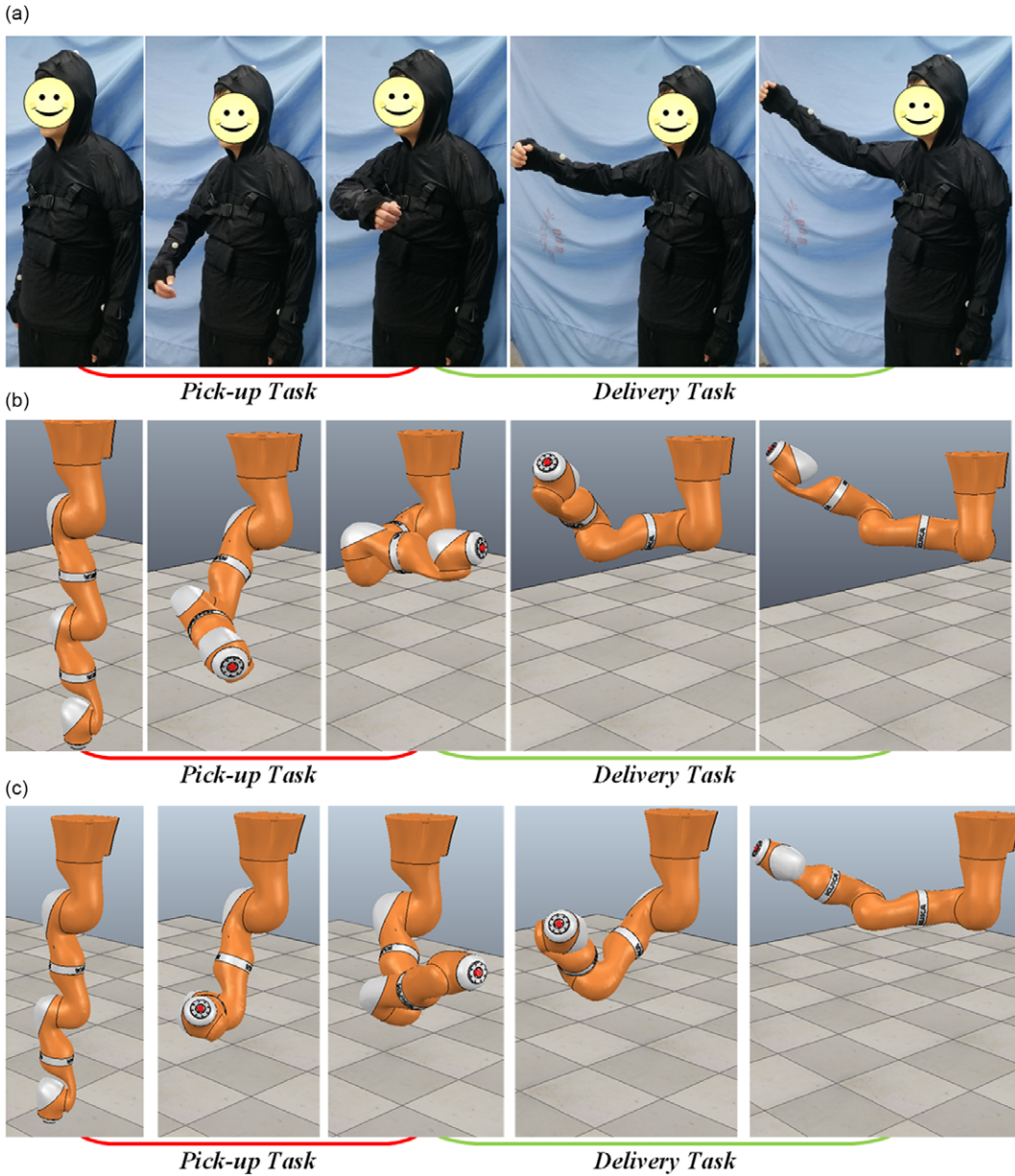


Figure 9. The human arm object handover task is in (a). The object handover task of the robot arm based on HMP method proposed in this paper is (b). The object handover task of the robot arm based on MTPE human-like motion planning method is (c).

HMP method proposed in this paper is slightly different from the human arm pose. In contrast, the robot posture based on MTPE method significantly differs from the human arm pose. Because MTPE method to make the robot always maintain the minimum energy posture, resulting in a significant difference from the human arm posture.

After calculating the motion data, RULA scores of the big arm, forearm and wrist when the human arm, and the robotic arm complete the object handover task are obtained, as shown in Fig. 10(a)–(c).

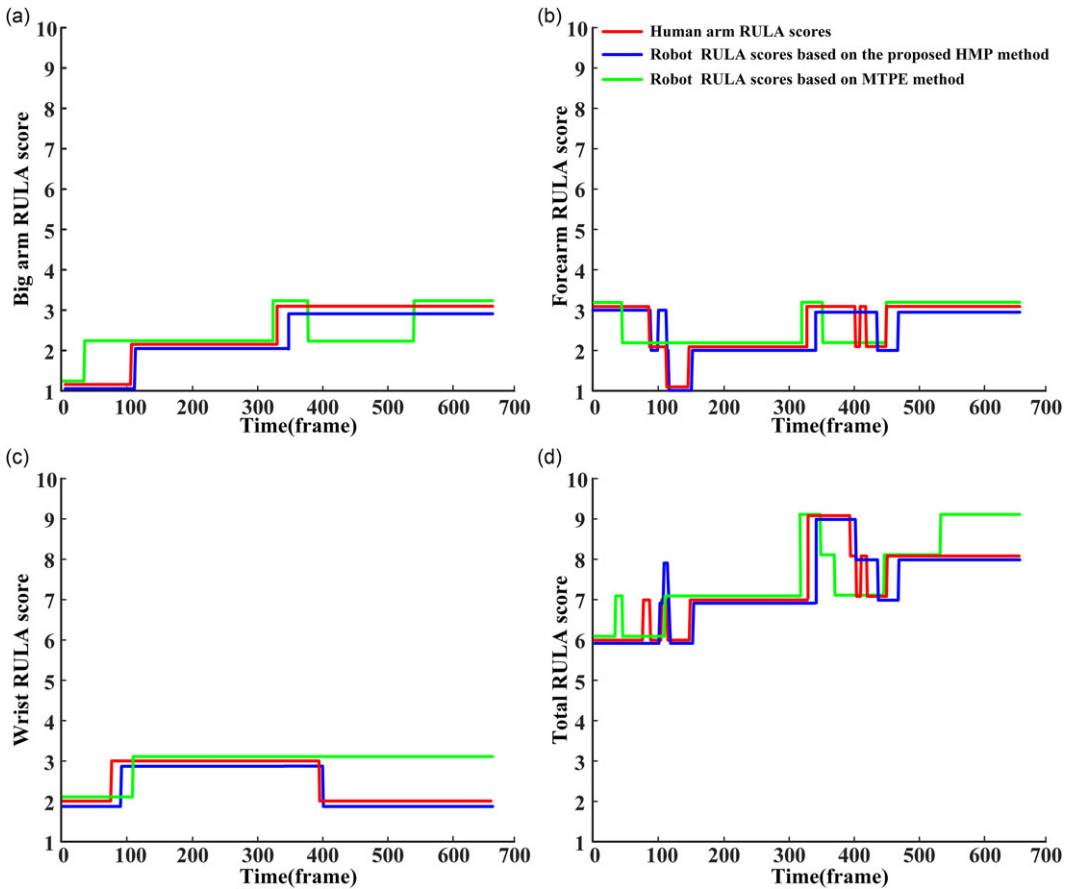


Figure 10. RULA score changes during object handover motion. RULA scores of the big arm, forearm, and wrist of the human arm and robotic arm are in (a), (b), and (c), respectively. The total RULA score of the human arm and robotic arm is shown in (d). The red curve shows RULA trend of the human arm. The blue curve shows RULA change trend of the robot based on the proposed motion planning method. The green curve shows RULA change trend of the robot based on MTPE planning method.

Figure 10(d) shows the total RULA scores of the human and the robotic arms obtained by adding the big arm, forearm, and wrist scores. In Fig. 10, RULA scores from 0 to 300 frames are RULA scores in the pick-up task of the human arm and robotic arm, and RULA scores from 300 to 700 frames are RULA scores in the delivery task of the human arm and robotic arm. Figure 10 shows that for the motion generated by the proposed algorithm, the changing trend of the robot’s RULA score and RULA score are similar to those of the human arm. RULA scores and trends of the robot arm, forearm, and wrist are identical to those of the human arm. It shows that HMP method proposed in this paper can achieve the purpose of the human-like motion of the robot. For the motion generated by MTPE method, the robot’s RULA total score and change trend are different from the human arm’s RULA total score and change trend. In addition, RULA scores and trends of the robot arm, forearm, and wrist differ significantly from those of the human arm, forearm, and wrist. It can be seen from RULA scoring rules that RULA scoring and changing trend of the robot and human arms differ significantly due to the significant difference between the robot posture and the human arm posture. In conclusion, the proposed HMP method is superior to MTPE method in HMP. Therefore, HMP method in this paper can help humans better understand and interpret the robot’s intention, which can improve the quality of the human-robot interaction.

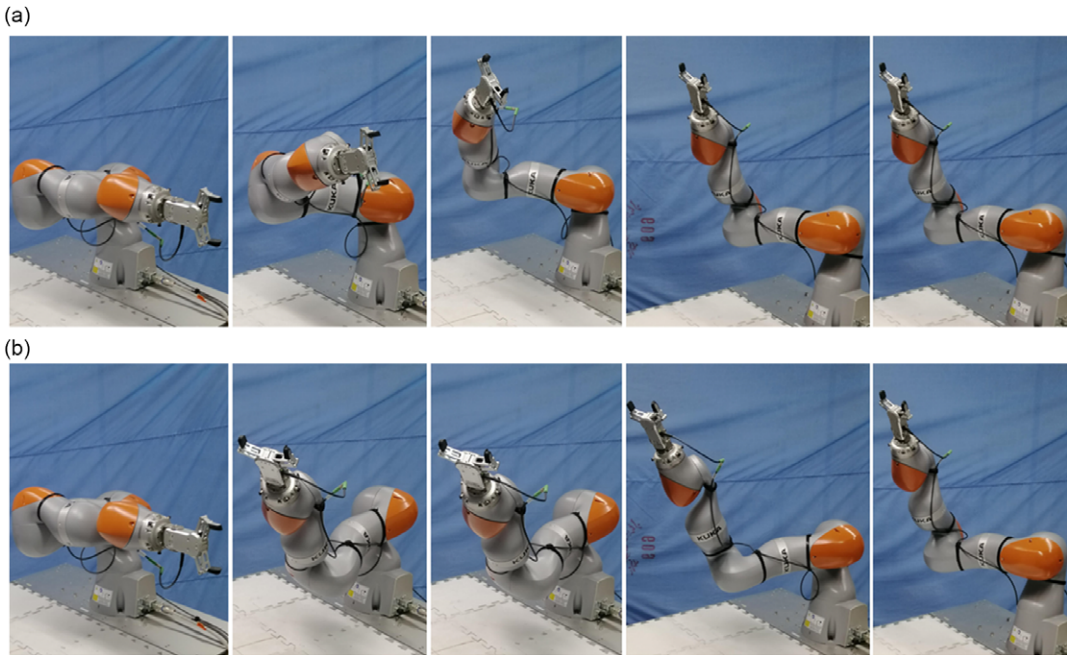


Figure 11. The proposed motion planning method experiment is shown in (a). MTPE planning method experiment is shown in (b).

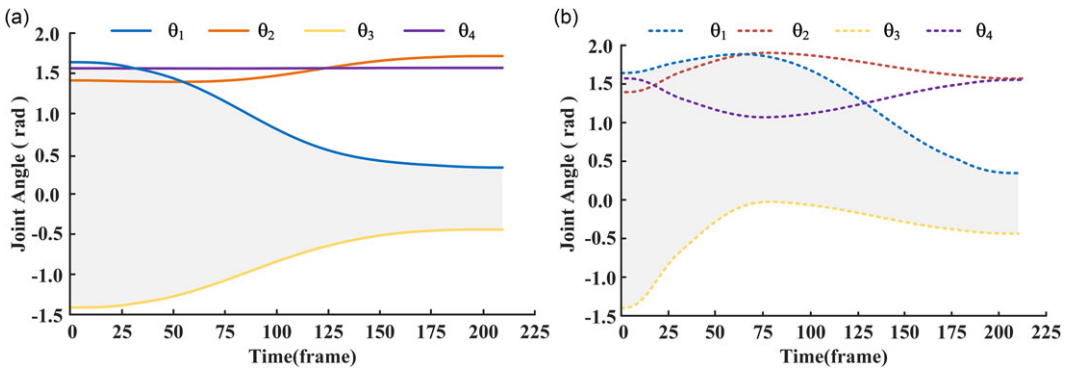


Figure 12. The first four joint trajectories of the proposed motion planning method are shown in (a). The first four joint trajectories of MTPE planning method are shown in (b).

To study the influence of HAMPs on the robotic arm’s motion, the delivery task of the object handover is computed by using the proposed method and MTPE method in ref. [7]. In the two planning methods, the robotic arm’s initial posture is the same, and the target posture is the same, as shown in Fig. 11.

The first four joint trajectories generated by the two motion planning methods are shown in Fig. 12. The joint trajectories obtained by the two motion planning methods are quite different. For example, the motion trajectory of joint one obtained by MTPE motion planning method had obvious peaks, which may be caused by the method making the robotic arm reach the MTPE as quickly as possible during the motion. The shapes of the shadowed area between the trajectories of the joints can be used to represent the relative relationship between the joints. For example, the shape of the shaded area formed by joints 1 and 3, in Fig. 12. Figure 12 shows that the regional shapes of the joint trajectories obtained by the

two planning methods are significantly different. Therefore, the relative relationship between the joints obtained by the different planning methods is also different.

7. Conclusion

The paper developed HMP method based on HAMPs for the robotic arms. By studying the human arm motion during the object handover, MPCSI is established to select HAMPs that can represent the motion characteristics of the arm in each motion phase of the pick-up and deliver sub-tasks. HAMPs selected from the first and the second motion phases in the pick-up subtask are Φ PO and Φ PO-PO, respectively. The first-phase HAMPs selected in the delivery subtask are Φ PO and PO- Φ PO, and the second-phase motion phase selected is Φ PO and Φ PO-PO. The studies of the primitive duration show that the primitive P and O duration is approximately equal to the total duration. The duration of the primitive Φ increases with the increase of the parameter R_d , so the duration of the primitive Φ can be estimated by the parameter R_d . Based on the selected HAMPs and the duration of the movement primitives, HMP method is established. The experimental results show that the proposed motion planning method can generate motion very close to actual human arm motion. In future work, we will study the human-like motion of the robot when there is an interaction force and further improve the effectiveness and efficiency of the human–robot interaction.

Acknowledgments. This work was supported by the National Natural Science Foundation of China (No. 51975008).

Conflicts of interest. No conflict of interest exists in the submission of this manuscript, and manuscript is approved by all authors for publication.

References

- [1] H. Su, W. Qi, Y. Hu, H. R. Karimi and G. Ferrigno, “An incremental learning framework for human-like redundancy optimization of anthropomorphic manipulators,” *IEEE Trans. Ind. Inform.* **18**(3), 1864–1872 (2022).
- [2] S. Yun, “A gaze control of socially interactive robots in multiple-person interaction,” *Robotica* **35**(11), 2122–2138 (2017).
- [3] T. Flash and N. Hogan, “The coordination of arm movements: An experimentally confirmed mathematical model,” *J. Neurosci.* **5**(7), 1688–1703 (1985).
- [4] Y. Uno, M. Kawato and R. Suzuki, “Formation and control of optimal trajectory in human multijoint arm movement,” *Biol. Cybern.* **61**(2), 89–101 (1989).
- [5] B. Almasri and F. B. Ouezdou, “Human-Like Motion Based on A Geometrical Inverse Kinematics and Energetic Optimization,” *In: 2008 IEEE/RSJ International Conference on Intelligent Robots and Systems* (2008) pp. 640–646.
- [6] M. Kittaka, A. Furui and H. Sakai, “Spatiotemporal parameterization of human reaching movements based on time base generator,” *IEEE Access* **8**, 1044–1055 (2020).
- [7] J. Zhao, B. Xie and C. Song, “Generating human-like movements for robotic arms,” *Mech. Mach. Theory* **1**(87), 107–128 (2014).
- [8] G. Gulletta, E. C. E. Silva and W. Erlhagen, “A human-like upper-limb motion planner: generating naturalistic movements for humanoid robots,” *Int. J. Adv. Robot. Syst.* **18**(2), 90–103 (2021).
- [9] M. Li, W. Guo, R. Lin, C. Wu and L. Han, “An efficient motion generation method for redundant humanoid robot arm based on the intrinsic principles of human arm motion,” *Int. J. Human. Rob.* **15**(6), 1–20 (2018).
- [10] M. Skubic and R. A. Volz, “Acquiring robust, force-based assembly skills from human demonstration,” *IEEE Trans. Robot. Autom.* **16**(6), 772–781 (2000).
- [11] R. Zoliner, M. Pardowitz and S. Knoop, “Towards Cognitive Robots: Building Hierarchical Task Representations of Manipulations From Human Demonstration,” *In: Proceedings of the 2005 IEEE International Conference on Robotics and Automation* (2005) pp. 1535–1540.
- [12] A. Yang, Y. Chen, W. Naem, M. Fei and L. Chen, “Humanoid motion planning of robotic arm based on human arm action feature and reinforcement learning,” *Mechatronics* **78**(3), 100–112 (2021).
- [13] C. Gabert, S. Kaden and U. Thomas, “Generation of Human-Like Arm Motions Using Sampling-Based Motion Planning,” *In: IEEE/RSJ International Conference on Intelligent Robots and Systems (IROS)* (2021) pp. 2534–2541.
- [14] T. Yu, “One-shot imitation from observing humans via domain-adaptive meta-learning,” *Proc. Robot. Sci. Syst.* (2018) pp. 1–4.
- [15] A. Sasagawa, K. Fujimoto, S. Sakaino and T. Tsuji, “Imitation learning based on bilateral control for human–robot cooperation,” *IEEE Robot. Automat. Lett.* **5**(4), 6169–6176 (2020).

- [16] A. Giuseppe, “Unveiling the principal modes of human upper limb movements through functional analysis,” *Front. Robot. AI* **4**(37), 110–124 (2017).
- [17] G. Averta, C. D. Santina and Valenza G, “Exploiting upper-limb functional principal components for human-like motion generation of anthropomorphic robots,” *J. Neuroeng. Rehabil.* **17**(1), 312–326 (2020).
- [18] X. Ding and C. Fang, “A novel method of motion planning for an anthropomorphic arm based on movement primitives,” *IEEE/ASME Trans. Mechatron.* **18**(2), 624–636 (2013).
- [19] C. Fang and X. Ding, “A2ML: A general human-inspired motion language for anthropomorphic arms based on movement primitives,” *Robot. Auton. Syst.* **1**(2), 145–161 (2019).
- [20] S. Gong, Z. Zhang and B. Xie, “Task motion planning for anthropomorphic arms based on human arm movement primitives,” *Ind. Robot.* **4**(5), 669–681 (2020).
- [21] G. Shiqiu, “Robot Motion Planning with Human-Like Motion Patterns Based on Human Arm Movement Primitive Chains,” **In: 2021 IEEE International Conference on Robotics and Automation (ICRA)**, Xian (2021) pp. 6281–6288.
- [22] P. Zhang and J. X. Zhang, “Motion generation for walking exoskeleton robot using multiple dynamic movement primitives sequences combined with reinforcement learning,” *Robotica* **40**(8), 2732–2747 (2022).
- [23] J. Zhao and C. Y. Wang, “Motion pattern of human arm reaching point movements based on the movement primitives,” *J. Mech. Eng.* **57**(19), 70–78 (2021).
- [24] S. Zhang, “Research on String Similarity Algorithm Based on Levenshtein Distance,” **In: 2017 IEEE 2nd Advanced Information Technology, Electronic and Automation Control Conference (IAEAC)** (2017) pp. 2247–2251.
- [25] D. Pesu and Z. Q. Zhou, “A Monte Carlo Method for Metamorphic Testing of Machine Translation Services,” **In: 2018 IEEE/ACM 3rd International Workshop on Metamorphic Testing (MET)** (2018) pp. 38–45.
- [26] Y. Wei, “Designing human-like behaviors for anthropomorphic arm in humanoid robot NAO,” *Robotica* **38**(7), 1205–1226 (2020).
- [27] I. S. Mackenzie, “Fitts’ law as a research and design tool in human-computer interaction,” *Hum-Comput. Interact.* **7**(1), 91–139 (1992).
- [28] N. Suwalee, P. Ru Ng Thip, N. M. Swangnetr, C. Sunisa, B. Rose and T. Stoffregen, “Ergonomic risk assessment of smartphone users using the Rapid Upper Limb Assessment (RULA) tool,” *PLoS ONE* **13**(8), 1–16 (2018).